

# RSC Advances



This is an *Accepted Manuscript*, which has been through the Royal Society of Chemistry peer review process and has been accepted for publication.

*Accepted Manuscripts* are published online shortly after acceptance, before technical editing, formatting and proof reading. Using this free service, authors can make their results available to the community, in citable form, before we publish the edited article. This *Accepted Manuscript* will be replaced by the edited, formatted and paginated article as soon as this is available.

You can find more information about *Accepted Manuscripts* in the [Information for Authors](#).

Please note that technical editing may introduce minor changes to the text and/or graphics, which may alter content. The journal's standard [Terms & Conditions](#) and the [Ethical guidelines](#) still apply. In no event shall the Royal Society of Chemistry be held responsible for any errors or omissions in this *Accepted Manuscript* or any consequences arising from the use of any information it contains.

## Microstructure and properties of carbon nanosheet/copper composites processed by particle-assisted shear exfoliation

Lidong Wang<sup>a,b</sup>, Ye Cui<sup>a</sup>, Shuai Yang<sup>a</sup>, Bin Li<sup>a</sup>, Yuanyuan Liu<sup>a</sup>, Pei Dong<sup>b</sup>, James Bellah<sup>b</sup>, Guohua Fan<sup>a</sup>, Robert Vajtai<sup>b,\*</sup> and Weidong Fei<sup>a,c,\*</sup>

<sup>a</sup> School of Materials Science and Engineering, Harbin Institute of Technology, Harbin, China, 150001

<sup>b</sup> Department of Materials Science and Nano Engineering, Rice University, Houston, Texas, United States, 77005

<sup>c</sup> School of Mechanical Engineering, Qinghai University, Xining, China, 810016

### ABSTRACT

The aim of this work is to demonstrate a facile and scalable method to produce carbon nanosheets (CNSs) based composites. CNSs and copper composite powders were produced directly from graphite and copper particles in liquids using a high shear rotor-stator mixer, the method is called particle-assisted shear exfoliation (PASE). CNSs reinforced copper composites were produced with the composite powders by spark plasma sintering (SPS). High strengthening efficiencies of CNSs in copper matrix composites were found, which are similar with those of carbon nanotubes. The interfacial microstructure of the composites was studied; a close contact between carbon and copper was obtained in the composite, which contributes to the mechanical property of the composites. PASE is also promising to produce many other kinds of composites by choosing numerous other layered crystals and nanomaterial particles.

*Keywords:* graphene; carbon nanosheets; composite; copper; exfoliation.

---

Corresponding authors:

Tel: +86 451 86418647 (W.D. Fei), +1 713-348-5904 (R. Vajtai).

E-mail addresses: wdfei@hit.edu.cn (W.D. Fei), Vajtai@rice.edu (R. Vajtai).

## Introduction

Carbon nanosheet (CNS, which includes single-layer graphene, few-layer graphene (FLG) and graphite nanosheet with a thickness less than 100 nm) are promising to revolutionize the research and applications of nano carbon based materials in the near future,<sup>1-3</sup> due to their outstanding chemical, mechanical, electrical and thermal properties.<sup>4,5</sup> Many methods have been developed to produce graphene and CNS, such as micromechanical cleavage of graphite<sup>1</sup>, chemical vapor deposition (CVD),<sup>6</sup> epitaxial growth on SiC,<sup>7,8</sup> exfoliation by sonication,<sup>9</sup> chemical oxidation and reduction method,<sup>10-11</sup> self-propagating high-temperature synthesis,<sup>12</sup> conventional calcination,<sup>13</sup> reduction of CO<sup>14</sup> and CO<sub>2</sub> (dry ice),<sup>15</sup> unzipping of carbon nanotubes<sup>16,17</sup> and laser reduction of graphene oxide.<sup>18-21</sup> The excellent properties of graphene make it an excellent candidate as the reinforcement of different kinds of composites,<sup>22,23</sup> which could be used in a wide range of fields such as catalyst,<sup>24</sup> battery,<sup>25</sup> supercapacitor<sup>26</sup> and nanocomposites.<sup>2</sup>

CNS reinforced polymer matrix composites have attracted more attention since 2006; their properties, such as electrical conductivity, Young's modulus and tensile strength, were remarkably improved by a low loading of CNS.<sup>2,27-29</sup> CNSs also show dramatically effects on the enhancement of the fracture toughness and conductivity of the CNS reinforced ceramic matrix composites.<sup>30-32</sup> Recently, graphene reinforced metal matrix composites demonstrate extraordinary reinforcement ability; Kim et al.<sup>33</sup> produced nanolayered graphene reinforced metal composites with ultra-high strength up to 1.5 GPa for copper matrix composite and 4.5 GPa for nickel matrix composite.

Hwang et al.<sup>34</sup> fabricated successfully CNS/Cu composites with the help of a molecular-level mixing method (MLM), remarkably improvement of the composite strengths was found. Consequently, different kinds of graphene and CNS based composites have shown great improvements on the multiple properties of the composites.

Generally speaking, the production of CNS/metal composites is not as easy as the polymer matrix composites. Because graphene oxide usually used in polymer matrix composites is easy to be produced in large scale, distributed homogeneously in solution and decorated with different groups which help to link with the groups of polymer and adjust the properties of the composites. However, the techniques used in CNS/metal composites are more difficult compared with those used for polymer matrix composites. For example, the nanolayered metal matrix composites have strict requirements for equipment and process;<sup>33</sup> the production of the composites by MLM method needs a long process including the production of graphene oxide, the distribution of graphene oxide into the solution of copper salt, drying, reducing and sintering processes of the composite powder.<sup>34</sup> So it is still a great challenge to develop simple and mass production methods for CNS/metal composites. However, there are few studies on this field, new methods should be developed for CNS based composites with practical value.

Shear mixing has already shown a broad application prospects in nanomaterials field. It is usually used to disperse nanoparticles in liquids by breaking up the nanoparticle agglomerates.<sup>35</sup> Recently, Paton et al.<sup>36</sup> pointed out that high-shear

mixing can also be used to exfoliate graphite into graphene in liquids. Shear mixing is useful to exfoliate directly untreated layered crystals in liquids using only high-shear mixer, which is different from the methods mentioned in a number of references for the exfoliation of graphite or layered compounds that incorporated shear mixing because treated layered crystal was first produced by intercalation to weaken the interlayer binding strength in these references.<sup>2, 32, 33, 37</sup>

Based on the reference<sup>36</sup> and our technique,<sup>38</sup> we produced successfully CNS/Cu composite powder directly from graphite and copper particles in liquids using shear mixing; since copper particles play an important role in the exfoliation process, the method is called particle-assisted shear exfoliation (PASE). The CNS/Cu composite powder was then consolidated into CNS/Cu composite by spark plasma sintering (SPS). High strengthening effect of CNS, high compressive strengths and good electrical conductivity were obtained simultaneously in the CNS/Cu composites. In our knowledge, it is the first time to produce CNS reinforced copper matrix composite with good properties from graphite and copper with 100 % use of the starting materials.

## **Experimental**

### *Sample preparation*

CNS/Cu composite powders were produced in our lab by mixing graphite and copper particles in liquid using a rotor-stator mixer. Commercial flake graphite (50  $\mu\text{m}$ , > 98%, Tianjin Bodi chemical holding Co., Ltd.), two kinds of copper particles (particle size 50 nm, Jiaozuo Banlu Nano Material Engineering Co., Ltd and particle

size 500 nm, Guangbo New Nanomaterials Stock Co., Ltd.) were dispersed in a solvent (ethyl alcohol, 1,3-propanediol or 1,3-butanediol) to obtain a slurry (the compositions were listed in Table 1). A rotor-stator mixer (BME200L, Shanghai Weiguang Machine Co. Ltd.) was used to treat the slurry in a vessel as shown in Fig. 1. The mixing head is a 4-blade rotor with a diameter of 35 mm that sits within a fixed screen known as the stator (the rotor-stator gap is  $\sim 100 \mu\text{m}$ ). The mixing speed is 3000 rpm. The treated slurry was centrifuged for 1 h with a speed of 8000 rpm to separate the composite powders from the solvent using a TG16G centrifuge (Hunan Kaida Technology Co. Ltd.). The composite powders were further heated at  $200 \text{ }^\circ\text{C}$  in air to remove the residual solvent after centrifugation.

Table 1. Slurry Compositions

Sample	Graphite [g]	Cu(50nm) [g]	Cu(500nm) [g]	Solvent [ml]
A	0.9375	0	150	500 (Ethyl alcohol)
B	0.9375	0	150	500 (1,3-Propanediol)
C	0.9375	0	150	500 (1,3-Butanediol)
D	0.9375	50	100	500 (1,3-Butanediol)

The composite powder D was reduced by  $\text{H}_2$  in a furnace at  $200 \text{ }^\circ\text{C}$  for 30 min. The composite, denoted as CNS/Cu(D), with a diameter of 20 mm and a length of 5 mm was sintered by SPS method from the  $\text{H}_2$ -reduced powder D in a graphite mold with an inside diameter of 20 mm at  $600 \text{ }^\circ\text{C}$  in the vacuum of 0.1 Pa under a die head pressure of 40 MPa for 5 min with a heating rate of  $100 \text{ }^\circ\text{C}/\text{min}$ . The weight percent of CNS in the composite is 0.6 wt.% and the volume fraction is 2.5vol.%. As a comparison, a pure copper sample was also produced by SPS in the same preparation conditions as the CNS/Cu composites.

### Characterization

Scanning electron microscopy (SEM) images of the composite powders were obtained on an FEI Quanta 200FEG SEM. Transmission electron microscopy (TEM) and high resolution transmission electron microscopy (HRTEM) images were obtained on an FEI Tecnai G2 F30 TEM operated at 300 kV. The TEM samples of the powders were prepared by dripping the dilute slurry of the composite powder on a micro grate. The TEM samples of the composites had a thickness of 30 micrometers and a diameter of 3 mm; an electron transparent thin area was obtained by making a small hole in the middle of the samples using an argon ion milling (Gatan 691 Precision Ion Polishing System). X-ray photoelectron spectroscopy (XPS) measurements were conducted with a K-alpha (Thermo Fisher) system for XPS measurement. Non-monochromatic Al K<sub>α</sub> radiation was operated under vacuum  $1.0 \times 10^{-8}$  mbar; the constant-pass energy mode is 50 eV with a step size of 0.1 eV for the C1s photoelectron line. Raman spectroscopy (532 nm excitation) was performed on a BWS435-532SY Raman spectroscopy. The phases of the composite powders and the composites were analyzed by X-ray diffraction (XRD) on a Philips X'Pert X-ray diffractometer with Cu K<sub>α</sub> radiation. Compressive test was performed by using an Instron 5500R All-purpose Electronic Tester with a crosshead speed of 0.5 mm/min in room temperature. The compressive samples have a cylindrical disc shape, with 3 mm in height and 3 mm in diameter. The loading directions are parallel to the squeezing direction of the specimens. The conductive property was tested by four probe method with a 2512B Low DC Resistance Tester (Suzhou Changsheng Electronic Technology Co., Ltd.). The samples for conductivity tests were cut into sheets, 17 mm in length, 5

mm in width and 0.2 mm in thickness. The direction of conductivity tests is vertical to the pressing direction of the specimens.

## Result and discussion

In order to investigate semi-quantitatively the influence of solvent on the thinning effect of graphite, the value of the intensity ratio of graphite (002) peak verse Cu (111) peak ( $I_{\text{graphite}(002)}/I_{\text{Cu}(111)}$ ) is used as an index, according to the XRD spectra of the composite powders. The reasons are as follows. (1) The intensity of copper is considered as a reference based on the fact that the contents of copper in composite powders are same before and after mixing. We measured the diameters of 100 spherical copper particles randomly in the SEM images before and after 16 h mixing, respectively; the mean sizes of spherical copper particles before and after mixing were calculated and were 579.4 nm and 545.9 nm, respectively. The average size of the copper particles after mixing is 6 % less than that of the particles before mixing, which is caused by the friction between particles during the mixing process. The result indicates that the diameter of copper particles were not changing much during the mixing process. (2) The peaks corresponding to graphite (002) and Cu (111) are the strongest peaks among the peaks of crystal graphite (PDF No.41-1478) and copper (PDF No.04-0836), respectively, which can give us more accurate information about the thickness of CNS sheets.

Fig. 2a shows the XRD curves of composite powders of A, B and C produced with different solvents treated at 3000 rpm for 8 h by the rotor-stator mixer. The viscosities of ethyl alcohol, 1,3-propanediol and 1,3-butanediol are 1.1<sup>39</sup>, 47.4<sup>39</sup> and

$96^{40}$  mPa·s, respectively. It is clear that the values of  $I_{\text{graphite}(002)}/I_{\text{Cu}(111)}$  shown in Fig. 2b corresponding to sample A, B and C decrease with the increase of solvent viscosity. It is surprising to find that the value of  $I_{\text{graphite}(002)}/I_{\text{Cu}(111)}$  is very weak for sample C, which means that graphite has been exfoliated so effectively that the peak of graphite (002) can hardly be detected by the XRD. This result indicates that 1,3-butanediol is the best solvent for graphite exfoliation among the three solvents. The XRD spectrum of sample D treated at 3000 rpm for 8 h is also shown in Fig. 2a, which is similar with that of sample C. The (002) peak of graphite for sample D is also invisible, which indicates that the exfoliation effect of graphite for sample D is similar with that for sample C. As a result, the regular layered structure of graphite is destroyed efficiently during the shear mixing process.

Representative SEM images of the composite powder D treated for 16 h are shown in Fig. 3a and 3b. Fig. 3a indicates that graphite has been exfoliated into thin graphite sheets like ruffled pages, representing that the method has a distinct exfoliation effect on flake graphite. Fig. 3b shows a transparent, crumpled and veil-like sheet with a diameter of  $\sim 10$   $\mu\text{m}$ , which suggests the PASE method could produce sheets with a large size. Part of the sheet embeds in the copper powder, suggesting that the copper particles can prevent CNSs from restacking.

Fig. 3c is the TEM image of the composite powder D, in which many stacked thin sheets can be seen. The selected area diffraction patterns (SADPs) of the multilayer sheets in the inset of Fig. 3c show sets of patterns, one of them is

demonstrated by white lines with a hexagonal structure, which illustrates that the sheets have good crystal structure.

HRTEM image of the composite powder D in Fig. 3d exhibits a thin CNS, which is about 8 layers and 2.84 nm in thickness. The interplanar distance is  $\sim 0.36$  nm, which is similar with that of graphite. Several pieces of graphene can be found just pointed by a white arrow in Fig. 3d, which offers a proof indicates that graphene could be exfoliated from the surface of graphite by PASE.

HRTEM is also used to classify the thickness of CNS in the composite powders. The thickness distribution of CNS edge was obtained by large number of HRTEM observations of the composite powder D treated for 8-72 h as shown in Fig. 3e. The number (N) of CNSs for the observations is 24. The thicknesses of CNSs are mainly within 20 nm, which are less than 60 layers of graphene, while around 61% of them are within 10 nm.

The Raman spectrum of the composite powder D in Fig. 3f demonstrates three primary features: a D band at  $\sim 1347$   $\text{cm}^{-1}$ , a G band at  $\sim 1578$   $\text{cm}^{-1}$  due to the two-fold degenerate  $E_{2g}$  mode at the zone centre, and a second-order D (2D) band at  $\sim 2710$   $\text{cm}^{-1}$ . It is generally accepted that the intensity ratio of the D band to G band ( $I_D/I_G$ ) in Raman reflects the defect concentration of carbonaceous materials, the lower the ratio, the less the defect concentration.<sup>41</sup> According to Fig. 3f, the  $I_D/I_G$  ratio for sample D is 0.14, which is much lower than that of reduced graphene oxide (RGO) ( $I_D/I_G=1.1$ )<sup>42</sup> and that of FLG produced by mild ball milling ( $I_D/I_G\approx 0.62$ ),<sup>43</sup> but higher than those of produced by CVD<sup>6</sup> and liquid-phase exfoliation<sup>9</sup> ( $I_D/I_G\approx 0$ ). As a result, the defect

concentration in CNSs is much lower than those in RGO and FLG produced by mild ball milling, but higher than those produced by CVD and liquid-phase exfoliation. This result is consistent with reference, in which high quality graphene has been produced from graphite in liquid by shear mixing.

Fig. 3f compares the Raman spectra of the composite powder and bulk graphite. It is interesting to see that the shape of 2D peak of the composite powder is different from that of graphite. For the 2D peak of graphite, the main peak is at  $2713\text{ cm}^{-1}$  and there is a clear “shoulder” on its left because two components ( $2D_1$  and  $2D_2$ ) exist in bulk graphite.<sup>44</sup> However, for the powder sample, the 2D peak is more symmetric and no obvious “shoulder” can be found. In addition, the full width at half maximum (FWHM) of 2D peak for the composite powder is  $\sim 75\text{ cm}^{-1}$  which is much larger than that of graphite ( $\sim 33\text{ cm}^{-1}$ ).

In our opinion, the disappearance of the “shoulder” and the wider FWHM of 2D peak are the result of the existence of CNSs in the composite powder. It is noted the 2D peak for graphene (especially less than 5 layers) is more symmetric than that of graphite. The 2D peak also shifts to lower wavenumber with the decrease in layer numbers of few-layer graphene.<sup>45</sup> According to TEM results, CNSs are composed of many sheets with thickness mainly less than 20 nm. The 2D peaks of CNSs with less layer numbers appear at lower wavenumber, which overlap with the peaks of CNSs with higher thickness and produce a wider 2D peak. They also cover the “shoulder” of the 2D peaks produced by thicker sheets (which is similar to graphite) in the CNSs.

As a result, the “shoulder” of 2D peak of the composite powder almost disappears and its FWHM is wider than that of graphite.

The inset in Fig. 3f is the XPS spectrum of C1s for the composite powder D treated for 72 h, the sample was etched by Ar for 120 sec before XPS measurement. The peaks located at 284.5 and 288.9 eV originate from the  $sp^2$  C-C and  $-O-C=O$  structure, respectively. The higher relative intensity of peak at 284.5 eV suggests that the  $sp^2$  C-C structure is well preserved after a long time shear exfoliation. And very small amount of carboxyl group ( $-O-C=O$ ) appeared after 72 hours' mixing. The oxygen-containing groups of the functionalities existed in CNS produced by PASE is about 2%, which is smaller than that of RGO in Cu matrix composite after  $H_2$  reducing at  $550^\circ C$  (12.9%)<sup>46</sup>.

These results indicate that graphite is successfully exfoliated to CNSs by PASE. The production and the dispersion of CNSs into copper particles are fulfilled in one step. The exfoliation process of graphite can be illustrated in Fig. 4. Firstly, the slurry before treatment is prepared by distributing graphite and copper particles in a solvent, as shown in Fig. 4a. Secondly, the slurry is treated in a rotor-stator mixer (Fig. 4b). The high speed rotation of the rotor sucks materials into the narrow gaps between the precision-engineered stator/rotor assembly, where graphite and copper particles are subjected to mechanical and hydraulic shear. When the rotating speed is 3000 rpm, the line speed of the rotor vs the stator is  $\sim 5.5$  m/s. As the rotor moves quickly, the slurry is forced to go through the narrow gap ( $\sim 100 \mu m$ ) between the rotor and the stator. During this process, the friction and impact from copper particles, the shear

stress and the possible cavitation in solvent act on graphite particles as demonstrated in Fig. 4b. The higher the solvent viscosity, the higher the shear stress of solvent on graphite, that is why the exfoliation effect of 1,3-butanediol is better than those of ethyl alcohol and 1,3-propanediol. The friction, impact and shear stress on graphite help to exfoliate graphite to CNSs. Graphite, CNSs and copper particles can go through the gaps for thousands of times. Thirdly, CNSs can be separated simultaneously by copper particles when they are exfoliated in solvent during PASE, so we not only produce CNSs from graphite but also solve the problem of distributing one nanomaterial into another one. This is the main advantage of PASE different from other methods for the production of the CNS/Cu composite powder. Finally, CNS/Cu composite powder (as shown in Fig. 4d) can be eventually obtained after centrifugation and heating.

We illustrated the potential of this method by using the CNS/Cu composite powders to produce CNS/Cu composites. The composite powders were consolidated by SPS method into CNS/Cu composites which are shown as the inset in Fig. 5a. The volume fraction of CNSs in the composites is 2.5%, assuming that there is no loss of carbon during PASE and SPS processes. The relative densities of CNS/Cu(D)-8h and CNS/Cu(D)-32h are 98.5% and 99.3%, respectively, suggesting that the composites are dense. High relative density means less concentration of macro pores or cracks, which is beneficial to improve the mechanical and electrical properties of the composites.

SEM of the surface of the CNS/Cu(D) composite eroded in 5 % HF for 5 minutes is shown in Fig. 5a. It can be found that many translucent thin sheets (marked by white arrows) distributed randomly in the composite. Because most of the copper on the surface is removed, and the image in Fig. 5a is a superposition image of the CNSs, so it seems that the content of CNS is far more than the actual content.

Fig. 5b shows the XRD spectra of the composites. The intensity of graphite (002) peak at 26.7 degree appears after sintering, which is invisible for composite powder after 8 h treatment (Fig. 2c). The result suggests that some of the thinner CNSs have recovered and become thicker ones during the process of SPS sintering. The little peak of  $\text{Cu}_2\text{O}$  (200) plane indicates weak oxidation happens in the composite. The inset in Fig. 5b shows the XPS spectrum of C1s for CNS/Cu(D) composite treated for 32 hours. The peak located at 284.5eV originates from the  $\text{sp}^2$  carbon, illustrating that  $\text{sp}^2$  carbon is the main type of carbon in the composite.

The fractography was shown in Fig. 5c. The sample for the fractography was prepared by breaking a thin sheet (about 0.5 in thickness, 2 in width, 4 in length) with tensile stress. A lot of CNSs were pulled out from the copper matrix. This result implies that plenty of CNSs exist in the composite, which could bear the load from copper matrix and be used to reinforce the copper composite.

High-Angle Annular Dark-Field (HAADF) was used to analyze the structure of the composite. The thin and dark crystal boundaries in Fig. 6a illustrate that materials with lower atomic number exist between the copper grains, as the contrast of HAADF image depends strongly on the average atomic number. The result of HAADF

strongly suggests that carbon distributes in the grain boundary of copper, since only copper, carbon and trace of oxide exist in the composite according to XRD result of the composite (Fig. 5b).

Fig. 6b shows the TEM of CNS/Cu(D) composite treated for 32 hours, Fig. 6c and 6d are the enlarged images of the red and green frame areas in Fig. 6b, respectively. Some carbon sheets and particles can be found among copper grains, especially, in triple grain boundary junctions in Fig. 6b-d; the thicknesses of the sheets are less than 10 nm as shown in Fig. 6c-f; the particles existing between grain boundaries are indicated by black arrows as shown in Fig. 6d. The HRTEM of the interface of copper and carbon are shown in Fig. 6e and 6f, there are no gaps or holes on the interface, indicating that the interface combination of copper and CNS is very good.

According to SEM and TEM observations, two types of CNS exist in the CNS/Cu composite. One is the isolated sheets with the size of several ten micrometers, which can be observed conveniently through SEM, as shown in Fig. 5a. The other is the smaller sheets existing in the copper grain boundary, especially, at the triple grain boundary junction, as shown in Figure 6, which can only be found through TEM observation.

The compact structure of the interface could contribute to the understanding of the interfacial bonding between CNS and copper. Hwang et al. have measured the adhesion energy between the graphene and Cu prepared by SPS, which is  $164 \pm 28.47 \text{ J}\cdot\text{m}^{-2}$ , and much greater than the adhesion energy of  $0.72 \pm 0.07 \text{ J}\cdot\text{m}^{-2}$  for as-grown

graphene on a Cu.<sup>34</sup> The origin of enhanced bonding strength between the graphene and metal was explained by the existence of native oxygen on Cu. However, no microstructure information was given in their work. Our work offers the microstructure information of the interface between CNS and copper, which suggests that beside the reason given in the reference<sup>34</sup> the compact structure of the interface may also contribute to the bonding strength of copper and CNS by mechanic occlude, beside the reason given in reference<sup>34</sup>.

The formation of the close integration interface may be related to the following factors. Firstly, a process of carbon diffusion-precipitation may happen during the process of SPS. Some of the carbon atoms at grain boundaries may diffuse into copper when the grain boundaries reach a higher temperature by the joule heat produced at the contact area during the process of SPS, and then they precipitate during the cooling process of the rapid multiple pulse cycle processes. Secondly, SPS has certainly shown the ability to achieve highly compacted bulk materials,<sup>47-49</sup> and the physical factors, such as the pulsed DC current and plasma, may facilitate the formation of the integration interface although the sintering mechanism of SPS has not been clearly understood thus far.<sup>50-52</sup>

The mechanical properties of the CNS/Cu composite were characterized using compressive tests. The compressive stress–strain curves of the composites and pure copper produced by SPS in the same preparation conditions are shown in Fig. 7a. The error bars were calculated by two specimens for each material. The compressive

behaviors of the CNS/Cu(D)-8h and CNS/Cu(D)-32h composites are similar, which indicates that 8 h is long enough to peel graphite into CNS.

It is worth noting that the CNS/Cu composites exhibit excellent mechanical properties. The yield strengths of several different kinds of copper composites are shown in Fig. 7b. It can be found that the yield stress of CNS/Cu(D) (476 MPa) is more than 1.7 times higher than that of pure copper (275 MPa) and also higher than those of copper composites enhanced by hybridized SiC and CNTs.<sup>53,54</sup>

It is interesting to see that an obvious strain hardening happened after yielding for the composites, while no obvious strain hardening could be found for pure copper (see shown in Fig. 7a). In our opinion, the strain hardening after yielding of the composites may be caused by the following reasons. Firstly, the dislocations produced during yielding process in the copper matrix can be repulsed by the boundary containing CNS when they move to the boundary, the repulsive force is called the image force and produced by the high modulus of CNS in the boundary.<sup>55</sup> The repulsive force blocks the dislocation motion. Secondly, when the dislocation pile-up takes place, it can be pinned effectively by the CNS in the grain boundary, as a result of high strength and modulus of the CNS. In addition, the deformation twins may also be restricted by hard CNS and high strength interfacial bonding. As a result, the strain hardening happened after yielding for the composites because of the existence of CNS in the grain boundary.

The strengthening efficiency of reinforcement  $R$  is an important parameter used to evaluate the effect of reinforcement in metal matrix, defined as the ratio of the

amount of yield strength increase of the composite to the actual yield strength of the matrix.<sup>35</sup>  $R$  is expressed as

$$R = (\sigma_c - \sigma_m) / V_f \sigma_m \quad (1)$$

where  $V_f$  is the volume fraction of reinforcement,  $\sigma_c$  is the yield strength of the composite and  $\sigma_m$  is the strength of the copper matrix (275MPa). The strengthening efficiencies of CNSs in composites have been calculated. One can find that the CNSs show high strengthening effect on copper composites. The strengthening efficiencies of CNSs in CNS/Cu(D) is 30.5, which is similar to that of CNTs in 5 vol.% CNTs/Cu composite and 1.5 times higher than that of CNTs in 10 vol.% CNT/Cu composite.

Four factors may play important roles for the improvement of the compressive strengths of the composites. Firstly, the successful fabrication of CNSs from graphite and the homogeneous distribution of CNSs in the composite guarantee the mechanical properties of the composites. Secondly, fine-grain strengthening may contribute to the strength of the composites according to the Hall-Petch relation, since the grain sizes of the composites are as small as several hundred nanometers. Thirdly, as indicated in reference,<sup>34</sup> the interfacial bonding of CNS and copper would be strong, which contributes to the stress transformation from the matrix to CNSs; so the strong interface benefits the strength of the composites. In addition, due to the high strength and flexibility, CNS can act as both the obstacle for dislocation propagation and the dislocation absorber for preventing dislocation pile-up, which can improve the strength of the composites.

The electrical conductivity values of the composites were measured and expressed as percent IACS. Here, IACS means International Annealed Copper Standard, a unit of electrical conductivity for metals and alloys relative to a standard annealed copper conductor; an IACS value of 100% refers to a conductivity of 58.0 MS/m at 20 °C. The conductivity value of CNS/Cu(D)-8h (81.0 %IACS) is higher than that of CNS/Cu(D)-32h (40.5 %IACS), this may be due to the impurities introduced during the longer production process.

Our work demonstrates that the PASE method can be successfully used to produce CNS/Cu composite with excellent mechanical and electrical properties directly from graphite and copper powder. It is reasonable to deduce that the method used in this work is promising to produce many other kinds of composites by choosing numerous other layered crystals (such as h-BN, MoS<sub>2</sub>, MoSi<sub>2</sub>, MoSe<sub>2</sub> and MoTe<sub>2</sub>) and matrix particles (including nano or submicro particles such as Ni, Fe, Al, Ti, Pt, Pd, MnO<sub>2</sub>, Ni<sub>2</sub>O<sub>3</sub>, Fe<sub>2</sub>O<sub>3</sub>, TiO<sub>2</sub>, Al<sub>2</sub>O<sub>3</sub>, MgO).

## Conclusions

CNS/Cu composite powders were produced by PASE from graphite and copper powder. The synthesis of CNSs with lower defect concentration and the dispersion of CNSs into copper particles are achieved simultaneously with 100 % use of the starting materials of graphite and copper powder. CNS/Cu composites were produced by SPS with the composite powders. Microstructure study demonstrated that close contact between CNS and copper was formed. High strengthening efficiencies of CNSs, high strength and good electrical conductivity were obtained in the composites. In addition,

PASE is promising to produce many kinds of composites by choosing numerous layered crystals and nanomaterials particles.

### Acknowledgements

The authors gratefully acknowledge the support from the National Basic Research Program of China (No.2011CB612200), China Scholarship Council (No.201206125006) and Harbin Key Technologies R&D Programme (2012DB2CP029). Robert Vajtai specially acknowledges funding from the DOD: Air Force Office of Scientific Research for the Project MURI: Synthesis and Characterization of 3D Carbon Nanotube Solid Networks, Award No.: FA9550-12-1-0035.

### References

1. K. S. Novoselov, A. K. Geim, S. V. Morozov, D. Jiang, Y. Zhang, S. V. Dubonos, I. V. Grigorieva and A. A. Firsov, *Science*, 2004, **306**, 666-669.
2. S. Stankovich, D. A. Dikin, G. H. B. Dommett, K. M. Kohlhaas, E. J. Zimney, E. A. Stach, R. D. Piner, S. T. Nguyen and R. S. Ruoff, *Nature*, 2006, **442**, 282-286.
3. S. H. Song, K. H. Park, B. H. Kim, Y. W. Choi, G. H. Jun, D. J. Lee, B. S. Kong, K. W. Paik and S. Jeon, *Adv Mater*, 2013, **25**, 732-737.
4. M. Segal, *Nat Nanotechnol*, 2009, **4**, 611-613.
5. M. T. Hung, O. Choi, Y. S. Ju and H. T. Hahn, *Appl Phys Lett*, 2006, **89**.
6. X. S. Li, W. W. Cai, L. Colombo and R. S. Ruoff, *Nano Lett*, 2009, **9**, 4268-4272.

7. T. Ohta, A. Bostwick, T. Seyller, K. Horn and E. Rotenberg, *Science*, 2006, **313**, 951-954.
8. C. Virojanadara, M. Syvajarvi, R. Yakimova, L. I. Johansson, A. A. Zakharov and T. Balasubramanian, *Phys Rev B*, 2008, **78**.
9. Y. Hernandez, V. Nicolosi, M. Lotya, F. M. Blighe, Z. Y. Sun, S. De, I. T. McGovern, B. Holland, M. Byrne, Y. K. Gun'ko, J. J. Boland, P. Niraj, G. Duesberg, S. Krishnamurthy, R. Goodhue, J. Hutchison, V. Scardaci, A. C. Ferrari and J. N. Coleman, *Nat Nanotechnol*, 2008, **3**, 563-568.
10. W. S. H. Jr. and R. E. Offeman, *J. Am. Chem. Soc.*, 1958, **80**, 1339-1339.
11. D. Li, M. B. Muller, S. Gilje, R. B. Kaner and G. G. Wallace, *Nat Nanotechnol*, 2008, **3**, 101-105.
12. Cn. Pat., 201210344115.3, 2012.
13. J. Zhao, Y. Guo, Z. Li, Q. Guo, J. Shi, L. Wang and J. Fan, *Carbon*, 2012, **50**, 4939-4944.
14. C.-D. Kim, B.-K. Min and W.-S. Jung, *Carbon*, 2009, **47**, 1610-1612.
15. A. Chakrabarti, J. Lu, J. C. Skrabutenas, T. Xu, Z. Xiao, J. A. Maguire and N. S. Hosmane, *Journal of Materials Chemistry*, 2011, **21**, 9491.
16. P. Kumar, L. S. Panchakarla and C. N. R. Rao, *Nanoscale*, 2011, **3**, 2127-2129.
17. D. V. Kosynkin, A. L. Higginbotham, A. Sinitskii, J. R. Lomeda, A. Dimiev, B. K. Price and J. M. Tour, *Nature*, 2009, **458**, 872-875.
18. P. Kumar, *Rsc Adv*, 2013, **3**, 11987-12002.

19. U. Maitra, H. S. S. R. Matte, P. Kumar and C. N. R. Rao, *Chimia*, 2012, **66**, 941-948.
20. P. Kumar, K. S. Subrahmanyam and C. N. R. Rao, *Mater Express*, 2011, **1**, 252-256.
21. P. Kumar, B. Das, B. Chitara, K. S. Subrahmanyam, K. Gopalakrishnan, S. B. Krupanidhi and C. N. R. Rao, *Macromol Chem Phys*, 2012, **213**, 1146-1163.
22. A. K. Geim and K. S. Novoselov, *Nat Mater*, 2007, **6**, 183-191.
23. Z. P. Chen, W. C. Ren, L. B. Gao, B. L. Liu, S. F. Pei and H. M. Cheng, *Nat Mater*, 2011, **10**, 424-428.
24. M. Y. Yen, C. C. Teng, M. C. Hsiao, P. I. Liu, W. P. Chuang, C. C. M. Ma, C. K. Hsieh, M. C. Tsai and C. H. Tsai, *J Mater Chem*, **2011**, 21, 12880-12888.
25. X. Zhao, C. M. Hayner, M. C. Kung and H. H. Kung, *Adv Energy Mater*, 2011, **1**, 1079-1084.
26. Y. M. He, W. J. Chen, X. D. Li, Z. X. Zhang, J. C. Fu, C. H. Zhao and E. Q. Xie, *Acs Nano*, 2013, **7**, 174-182.
27. T. Ramanathan, A. A. Abdala, S. Stankovich, D. A. Dikin, M. Herrera-Alonso, R. D. Piner, D. H. Adamson, H. C. Schniepp, X. Chen, R. S. Ruoff, S. T. Nguyen, I. A. Aksay, R. K. Prud'homme and L. C. Brinson, *Nat Nanotechnol*, 2008, **3**, 327-331.
28. K. M. F. Shahil and A. A. Balandin, *Nano Lett*, 2012, **12**, 861-867.
29. H. J. Salavagione, G. Martinez and M. A. Gomez, *J Mater Chem*, 2009, **19**, 5027-5032.

30. Y. C. Fan, L. J. Wang, J. L. Li, J. Q. Li, S. K. Sun, F. Chen, L. D. Chen and W. Jiang, *Carbon*, 2010, **48**, 1743-1749.
31. L. S. Walker, V. R. Marotto, M. A. Rafiee, N. Koratkar and E. L. Corral, *Acs Nano*, 2011, **5**, 3182-3190.
32. J. Liu, H. X. Yan and K. Jiang, *Ceram Int*, 2013, **39**, 6215-6221.
33. Y. Kim, J. Lee, M. S. Yeom, J. W. Shin, H. Kim, Y. Cui, J. W. Kysar, J. Hone, Y. Jung, S. Jeon and S. M. Han, *Nat Commun*, 2013, **4**.
34. J. Hwang, T. Yoon, S. H. Jin, J. Lee, T. S. Kim, S. H. Hong and S. Jeon, *Adv Mater*, 2013, **25**, 6724-6729.
35. R. Wengeler and H. Nirschl, *J Colloid Interf Sci*, 2007, **306**, 262-273.
36. K. R. Paton, E. Varrla, C. Backes, R. J. Smith, U. Khan, A. O'Neill, C. Boland, M. Lotya, O. M. Istrate, P. King, T. Higgins, S. Barwich, P. May, P. Puczkarski, I. Ahmed, M. Moebius, H. Pettersson, E. Long, J. Coelho, S. E. O'Brien, E. K. McGuire, B. M. Sanchez, G. S. Duesberg, N. McEvoy, T. J. Pennycook, C. Downing, A. Crossley, V. Nicolosi and J. N. Coleman, *Nat Mater*, 2014, **13**, 624-630.
37. D.W. Murphy, G.W.Hull, *J Chem Phys*, 1975, **62**, 973
38. Cn. Pat., 20101079119.1, 2010.
39. J. A. Dean, in Lange's Handbook of Chemistry. McGraw-Hill, Inc, 15th edn., 1998, vol. 5, pp. 92-93.
40. N. J. Rahway, in The Merck Index - Encyclopedia of Chemicals, Drugs and Biologicals, Merck and Co., Inc, 1989, pp. 239.

41. A. Eckmann, F. Alexandre, V. Ivan, D. Rebecca, C. Cinzia. *Phys Rev B*, 2013, **88**, 035426.
42. I. K. Moon, J. Lee, R. S. Ruoff and H. Lee, *Nat Commun*, 2010, **1**.
43. J. Y. Huang, H. Yasuda and H. Mori, *Chem Phys Lett*, 1999, **303**, 130-134.
44. R.P. Vidano, D.B. Fischbach, L.J. Willis, T.M. Loehr, *Solid State Commun*, 1981, **39**, 341-344.
45. A. C. Ferrari, J. C. Meyer, V. Scardaci, C. Casiraghi, M. Lazzeri, F. Mauri, S. Piscanec, D. Jiang, K. S. Novoselov, S. Roth and A. K. Geim, *Phys Rev Lett*, 2006, **97**.
46. L. D. Wang, Y. Cui, R.Y. Li, G.J. Cao, B. Li and W.D. Fei, *Acta Metall Sin*, 2014, **27**, 924-929.
47. M. Kubota, *J Alloy Compd*, 2007, **434**, 294-297.
48. O. Ohashi, *J Jpn Welding Soc*, 2000, **69**, 91.
49. G. Q. Xie, O. Ohashi, T. Yoshioka, M. H. Song, K. Mitsuishi, H. Yasuda, K. Furuya and T. Noda, *Mater Trans*, 2001, **42**, 1846-1849.
50. M. Omori, *Mat Sci Eng a-Struct*, 2000, **287**, 183-188.
51. G. Q. Xie, O. Ohashi, K. Chiba, N. Yamaguchi, M. H. Song, K. Furuya and T. Noda, *Mat Sci Eng a-Struct*, 2003, **359**, 384-390.
52. M. Zadra, F. Casari, L. Girardini and A. Molinari, *Powder Metall*, 2007, **50**, 40-45.
53. M. R. Akbarpour, E. Salahi, F. A. Hesari, A. Simchi and H. S. Kim, *Mat Sci Eng a-Struct*, 2013, **572**, 83-90.

54. S. I. Cha, K. T. Kim, S. N. Arshad, C. B. Mo and S. H. Hong, *Adv Mater*, 2005, **17**, 1377-1381.

55. K. F. Ha, in *Micro-Theory of Mechanical Properties of Metals*, Scientific Press, Beijing, 1982, vol. 2, ch. 12, pp. 91-92.

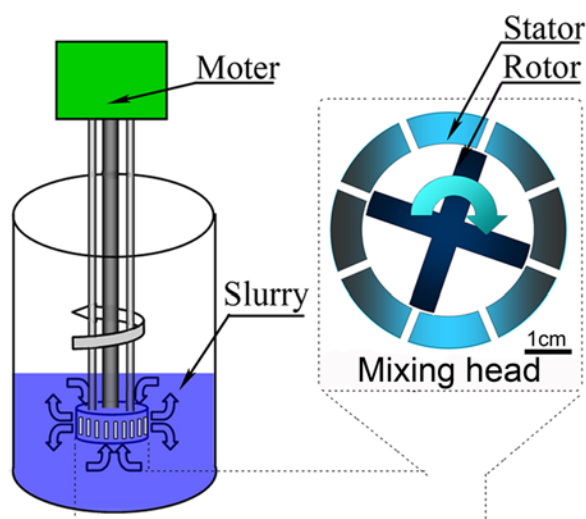


Fig. 1. Schematic illustration of experimental set-up.

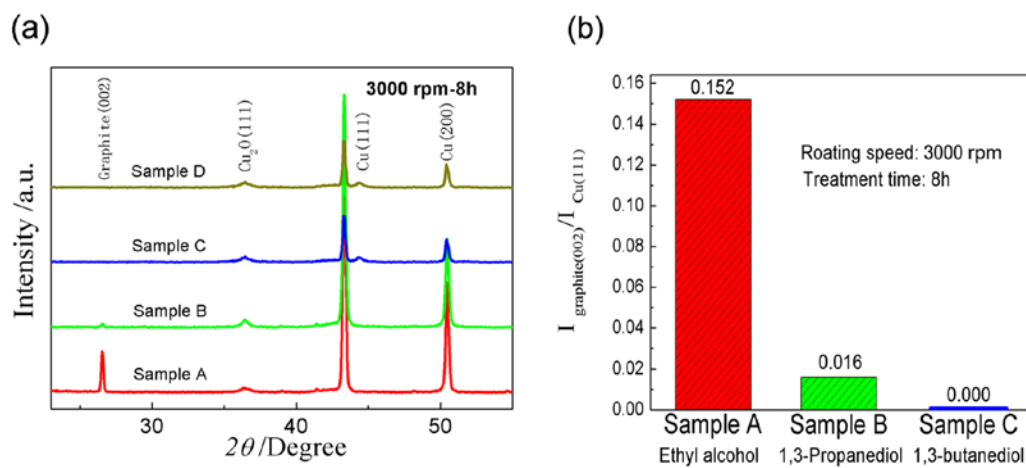


Fig. 2. (a) XRD spectra of composite powders corresponding to sample A, B, C and D; (b) Histogram of  $I_{\text{graphite}(002)}/I_{\text{Cu}(111)}$  corresponding to sample A, B and C.

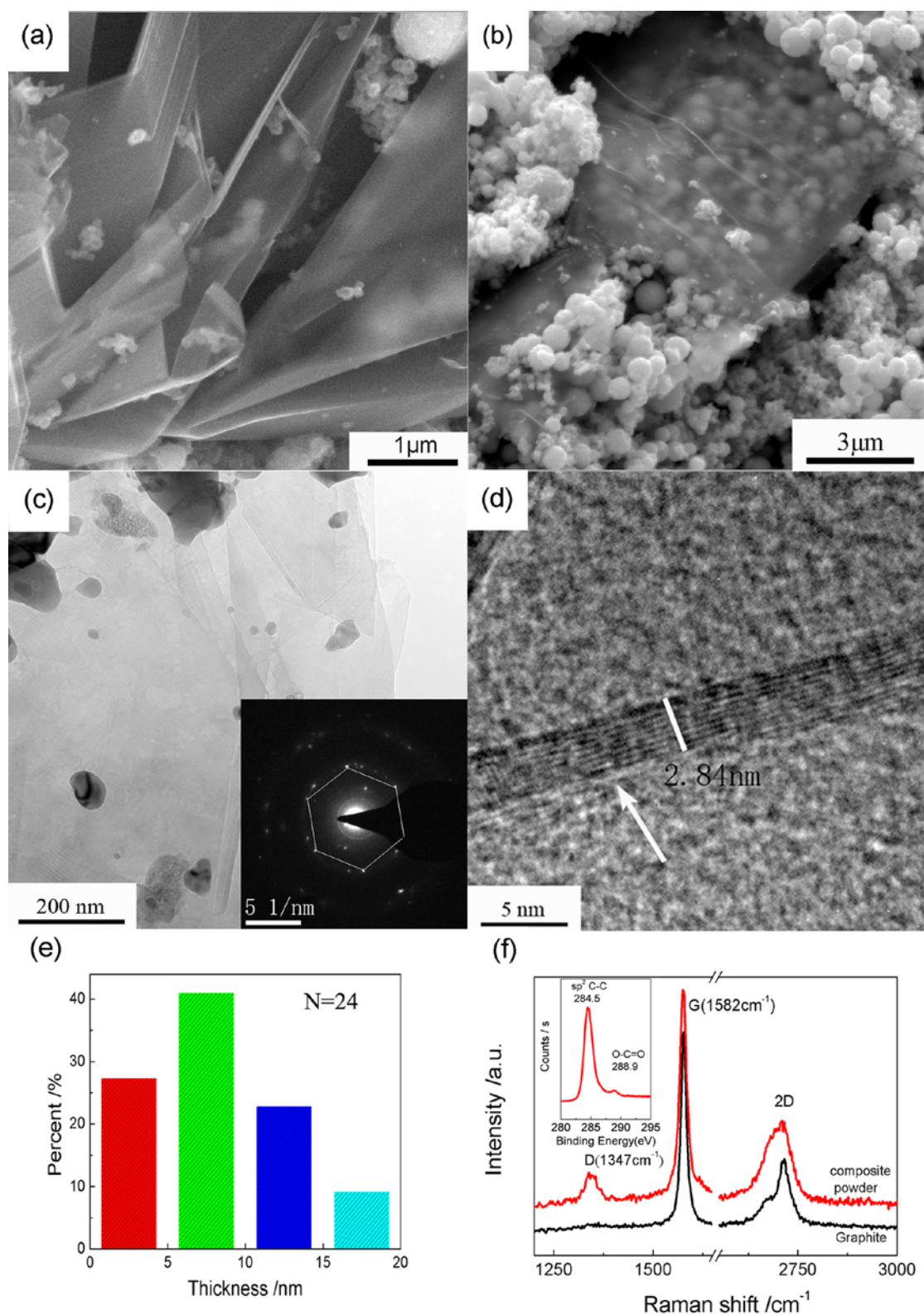


Fig. 3. a) Representative SEM image of some sheets look like ruffled pages; b) SEM image of a sheet like crumpled silk veil; c) TEM of the composite powder D with an insert SADPs (white lines were added to demonstrate the hexagonal structure of the diffraction pattern); d) HRTEM image of the CNS edges; e) Statistical chart of the sheets with different thickness, the “N” in image is the piece number of the sheets

observed; f) Representative raman spectra of composite powder D treated for 8 h and graphite. The inset is XPS of C1s spectrum of the composite powder D treated for 72 h.

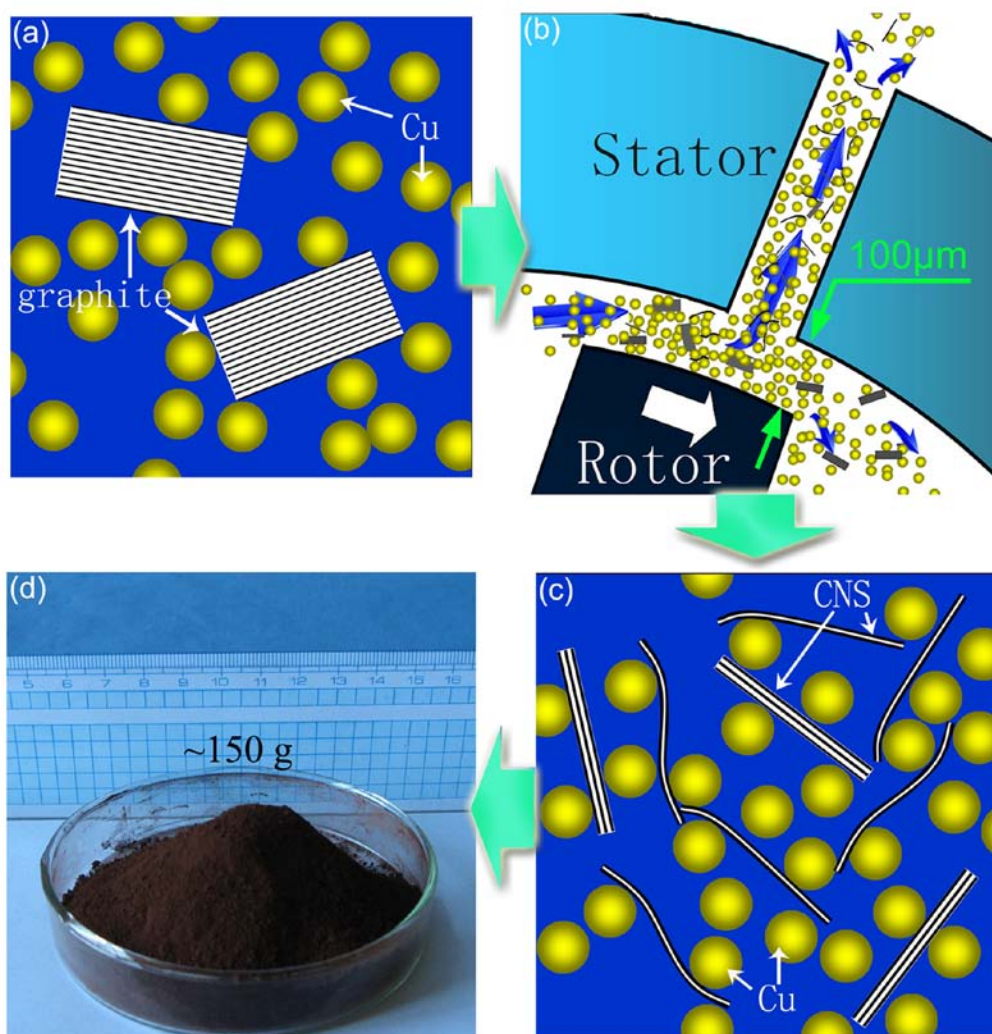


Fig. 4. Schematic illustration of PASE process: (a) Slurry before mixing treatment; (b) mixing treatment; (c) slurry after mixing treatment; (d) Photograph of CNS/Cu composite powder.

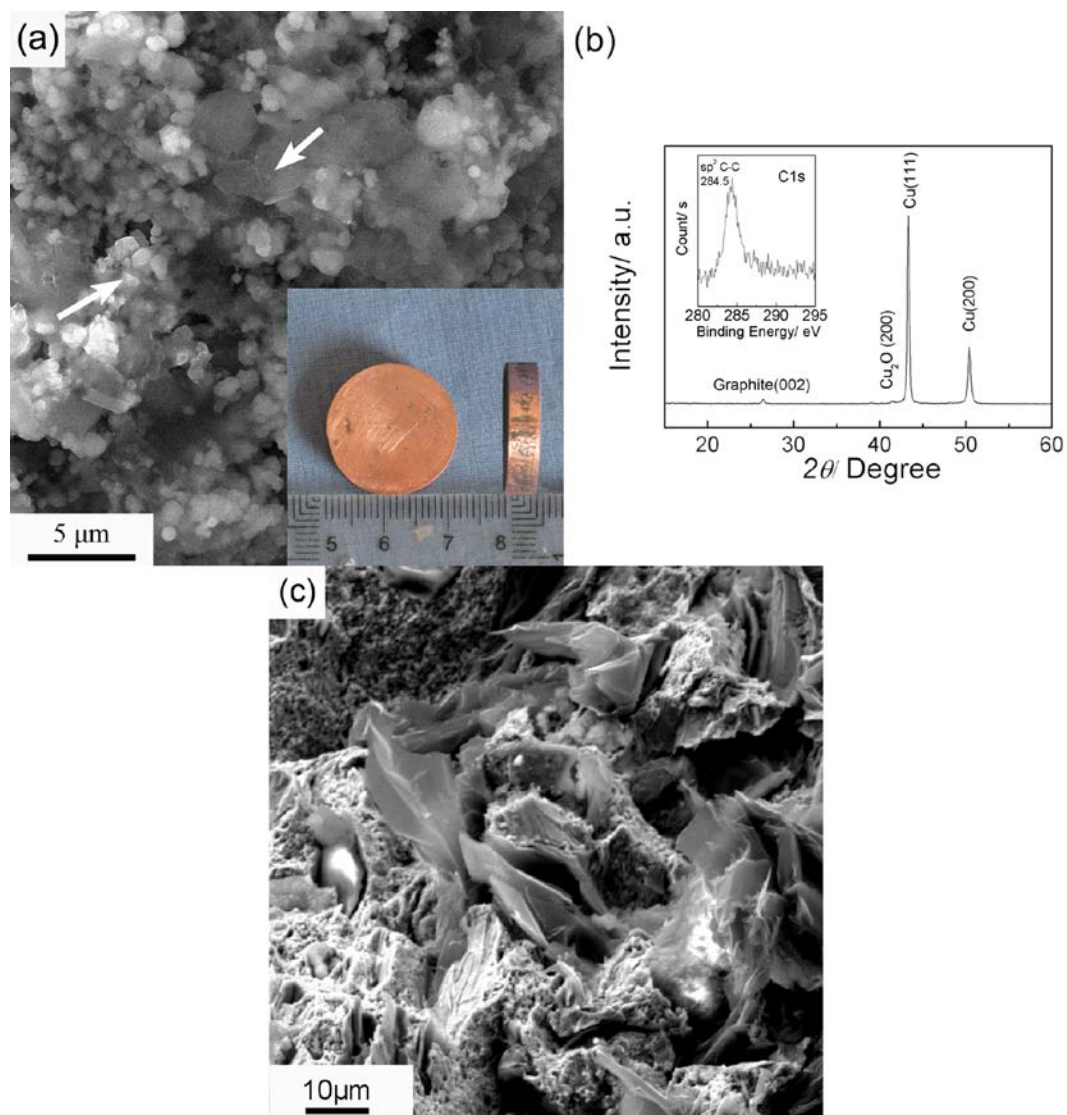


Fig. 5. (a) SEM morphology of the surface of the CNS/Cu(D) composite eroded in 5 % HF for 5 minutes, the inset shows the composite produced by SPS method; (b) XRD pattern of CNS/Cu(D) composite, the inset shows the C1s XPS of CNS/Cu(D) composite; (c) Fractography micrograph of the CNSs/Cu(D) composite.

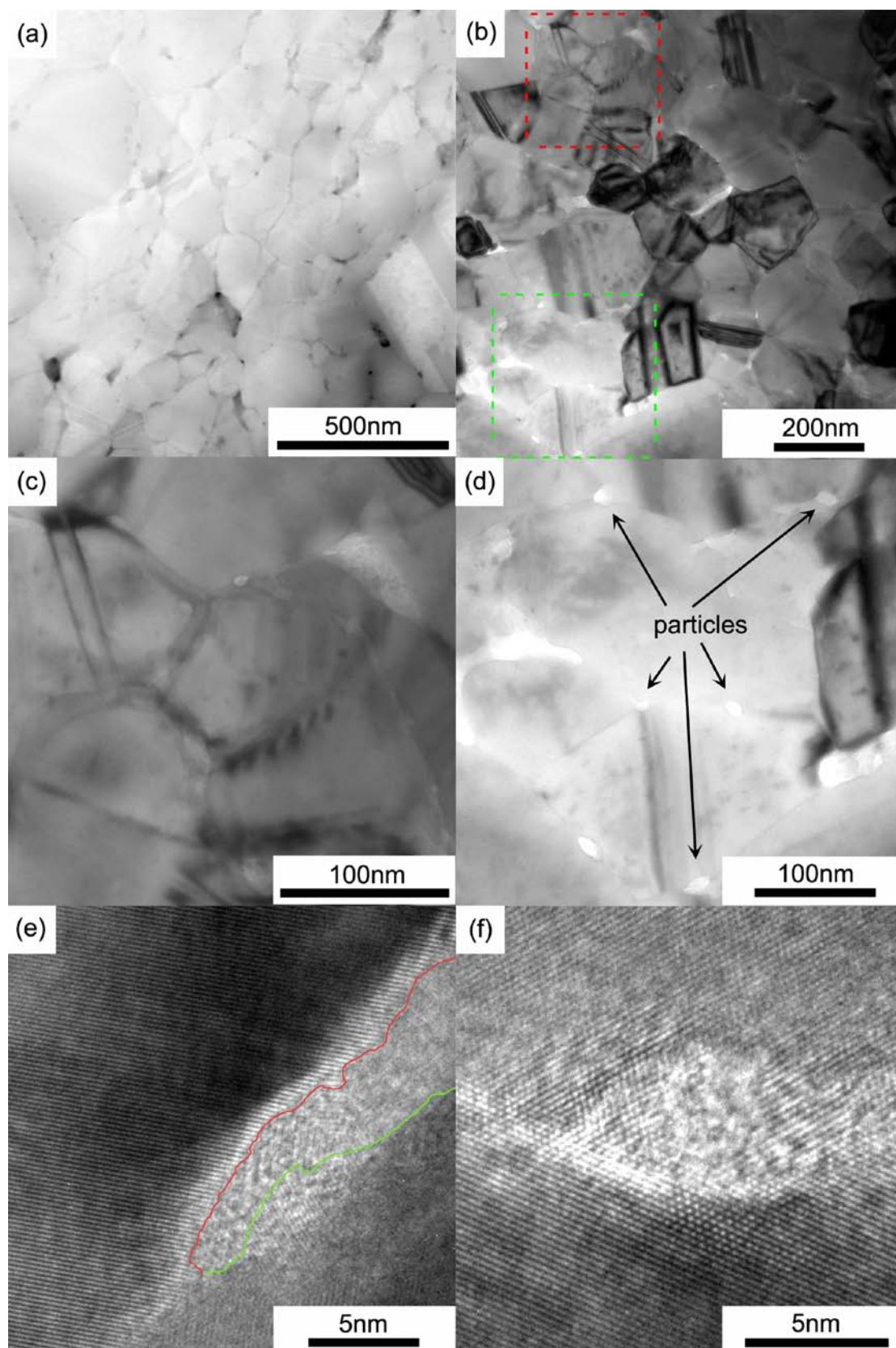


Fig. 6. Structure of CNS/Cu(D) composite treated for 32 hours: (a) HAADF image; (b) TEM image; (c) and (d) enlarged images from Fig. 6b; (e) and (f) HRTRM images of interfaces between carbon and copper.

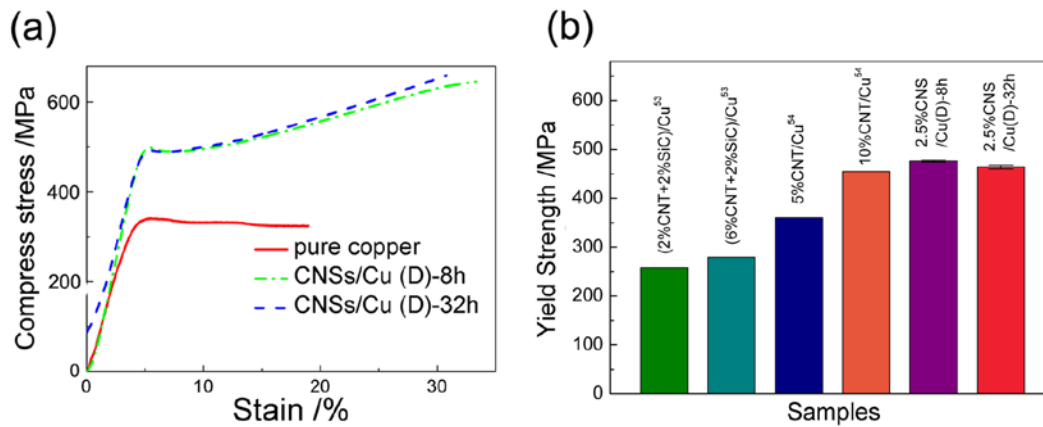


Fig. 7. (a) The compressive stress-strain curves of the composites and pure copper produced in the same conditions; (b) Comparison of yield strength of CNS/Cu(D) composite with 4 samples in references.<sup>53,54</sup>